A Letters Journal Exploring the Frontiers of Physics

January 2020

EPL, **129** (2020) 20001 www.epljournal.org
doi: 10.1209/0295-5075/129/20001

Many-body localization in generalized Kondo lattice with disorder

Ye Cao[1(a)] and Wei Zhang[2,3(b)]

[1] *School of Physics, Beijing Institute of Technology - Beijing 100081, China*
[2] *Department of Physics, Renmin University of China - Beijing 100872, China*
[3] *Beijing Key Laboratory of Opto-electronic Functional Materials and Micro-nano Devices, Renmin University of China - Beijing 100872, China*

received 10 December 2019; accepted in final form 29 January 2020
published online 14 February 2020

PACS 03.67.-a – Quantum information
PACS 05.30.-d – Quantum statistical mechanics
PACS 67.85.-d – Ultracold gases, trapped gases

Abstract – We study the many-body localization transition in a one-dimensional generalized Kondo lattice, where a one-dimensional Hubbard chain with disordered spin-orbit coupling interacts with a fixed impurity of spin 1/2. Using exact diagonalization, we characterize the many-body localized transition with entanglement entropy and energy spectrum distribution. We find that although the subsystem of the impurity is free of disorder, it can still be localized in the spin space by the coupling with the Hubbard chain. We also investigate the out-of-time-order correlation in the many-body localized phase, and find distinctive features in comparison to either the thermal state or the Anderson localized state. Our scheme can be realized in experiments with ultracold fermions of alkaline-earth–like atoms near an orbital Feshbach resonance.

Introduction. – The study of dynamical properties of disordered systems has been one of the key problems in condensed matter physics, ever since the publication of the seminal paper by Anderson in 1958 [1]. In that work, it is shown that a non-interacting system can undergo a quantum phase transition from transport to localized state for large enough disorder strength. In this so-called *Anderson localization* (AL) or *Anderson insulator* state, the particles interfere destructively and hence prevent transport in the thermodynamic limit. Following research proves that this phenomenon is more prominent in lower dimensions such that systems in one and two dimensions become an Anderson insulator in the presence of an arbitrarily small amount of disorder [2]. The absence of spreading of particle's wave-packet in AL phase implies the initial quantum information is permanently maintained, making it an ideal platform to produce quantum memory devices. However, in general, there is no purely isolated system. The coupling between the qubits and reservoirs essentially destroys the initial correlations in the quantum systems. Then how to eliminate the diffusion of quantum information from system to reservoir becomes a profound question.

Recently, the investigation of localization has been generalized to interacting systems, where a transition from transport to localized state can also be observed with increasing disorder both theoretically [3–14] and experimentally [15–18]. The localized state, referred to as *many-body localization* (MBL), is suggested to be a different state of matter with some distinct properties compared to either AL state or other interacting systems. For example, it is shown that, for an AL state, the entropy will first increase linearly with time and then nearly saturate to a constant after a sudden quench, while, for a MBL phase, the entropy will increase continuously with a logarithmic behavior for long enough time as a result of the interaction-induced dephasing [10,19]. Besides, the out-of-time-order correlator (OTOC) for an AL phase remains as a constant over time, but drops with a power-law dependence in a MBL phase [20]. More remarkably, it is known that the MBL phase does not satisfy the eigenstate thermalization hypothesis (ETH) [21–32], which means that the system does not thermalize even in the thermodynamic limit [33,34].

In this work, we study the MBL transition in a generalized Kondo lattice, where a one-dimensional (1D) Hubbard chain with disordered spin-orbit coupling couples to a fixed impurity of spin 1/2. Because of the presence of

(a) E-mail: 6120170047@bit.edu.cn
(b) E-mail: wzhangl@ruc.edu.cn

spin-orbit coupling, the impurity can be viewed as itinerant in the spin space, *i.e.*, can hop between the two spin eigenstates. This setup can be treated as a toy model to study whether the decoherence effect of environment in MBL on the system is weakened. Although the subsystem of the impurity does not acquire any apparent disorder, the randomness in the background Hubbard chain can induce a transition to the localized state and prevent hopping of the impurity in the space via the impurity-background coupling. To characterize the localized state, we numerically obtain the full spectrum by exact diagonalization (ED), and calculate various quantities that can distinguish a MBL state from either an AL state or a thermal state. Specifically, we evaluate the mean and standard deviation of the entanglement entropy of a subsystem, the average ratio of adjacent energy gaps, and the OTOC by varying the disorder strength. We also suggest that the model considered here can be implemented in ultracold Fermi gases of alkaline-earth–like atoms in 1D optical lattices and Raman-assisted spin-orbit coupling [35].

Model. – We consider a quasi-1D quantum gas of alkaline-earth–like atoms trapped in an optical lattice potential along the axial direction, and tightly confined in the transverse directions. In addition to the ground electronic state $^1S_0$, these two-electron atoms have a metastable state $^3P_0$, which is forbidden to couple with the ground state by dipole transition and hence acquires a very long lifetime in the scale of tens or even hundreds of seconds. Thus, for most experimental relevant cases, these two electronic states are considered to be stable and provide an additional degree of freedom referred to as orbital. In the following discussion, we label the $^1S_0$ state as orbital $|g\rangle$ and $^3P_0$ as orbital $|e\rangle$. As the total electronic angular momentum for both $|g\rangle$ and $|e\rangle$ orbitals is zero, the coupling between electronic and nuclear angular momenta is negligible and the different nuclear spin states are degenerate in the absence of magnetic field. For ^{87}Sr, the nuclear spin is 9/2, which gives 10 different Zeeman levels. While for ^{173}Yb, a nuclear spin of 5/2 gives 6 magnetic states. This nuclear spin degeneracy can be lifted in a finite Zeeman field. By selectively populating two of these nuclear spin states, we can then realize a spin-1/2 fermionic system where the nuclear spin states are labelled by (pseudo)spin $|\uparrow\rangle$ and $|\downarrow\rangle$.

A synthetic spin-orbit coupling between the two spin states within each orbital can be implemented via a Raman transition, as illustrated in fig. 1. Stimulated by the experimental scheme of Raman optical lattice [36], we assume one leg of the Raman transition in both orbitals is driven by a standing-wave with Rabi frequency $\Omega_{2,\alpha}(x) = \Omega_{2,\alpha}\cos(k_0x)$, where $\alpha = g, e$ labels different orbitals. The wave vector k_0 corresponds to the magic wavelength for ^{1}S$_0$ and ^{3}P$_0$ atoms. The other leg of the Raman transition is realized by a traveling wave $\Omega_{1,\alpha}(x)e^{ik_0x}$. While the magnitude of the $|g\rangle$ orbital $\Omega_{1,g}$ is a uniform constant, for $|e\rangle$ the orbital is assumed to be position-dependent and may acquire some disorder. As a result, the atoms in both orbitals are trapped in two 1D optical lattices, and are spin-orbit coupled with a uniform (random) intensity for the $|g\rangle$ ($|e\rangle$) orbitals. We stress that the intensities of the optical lattice potentials for the two orbitals can be varied independently since the AC polarizibilities are in general different.

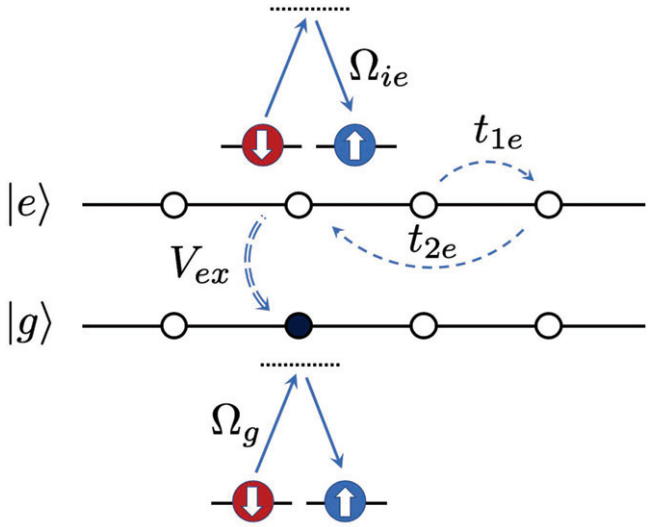

Fig. 1: Alkaline-earth–like atoms in the $|g\rangle$ and $|e\rangle$ orbitals are trapped in 1D optical lattices. With the aid of a Raman lattice, synthetic spin-orbit coupling can be implemented within both orbitals between different nuclear (pseudo) spin states. Near an orbital Feshbach resonance, the system features not only on-site Hubbard interaction, but also a spin-exchange interaction which couples the two orbitals as defined in eq. (3). The $|e\rangle$ orbital is quarterly filled, while the number of particle for the $|g\rangle$ orbital is fixed to be unity. Disorders are introduced to the $|e\rangle$ orbital solely. The atom in the $|g\rangle$ orbital is fixed in position to act as an immobile spinful impurity.

Within this setup, the single-particle Hamiltonian can be written as

$$\hat{H}_0 = \int \mathrm{d}x \sum_{\alpha\sigma} \hat{\psi}^\dagger_{\alpha\sigma}\left[-\frac{\hbar^2}{2m}\nabla^2 + V_\alpha(x) + \delta_{\alpha\sigma}\right]\hat{\psi}_{\alpha\sigma} + \int \mathrm{d}x \sum_{\alpha}[M_\alpha(x)\hat{\psi}^\dagger_{\alpha\uparrow}\hat{\psi}_{\alpha\downarrow} + \mathrm{H.c.}], \quad (1)$$

where $\sigma = (\uparrow, \downarrow)$, $\psi_{\alpha\sigma}$ is the annihilation operator for atoms with spin σ in the α orbital, and $\delta_{\alpha\sigma}$ denotes the differential Zeeman shifts under an external magnetic field. The lattice potential $V_\alpha(x) = -V_{0\alpha}\cos^2(k_0x)$, and the Raman potential $M_\alpha(x) = M_{0\alpha}(x)\cos(k_0x)$, where both V_0 and $M_{0\alpha}$ are proportional to the AC polarizability of the clock states. While the magnitude of the Raman potential for the $|g\rangle$ orbital $M_{0g}(x) = M_{0g}$ remains a constant, that for the $|e\rangle$ orbital is a random function $M_{0e}(x) = M_{0e}\mathrm{rand}(0, 1)$ with amplitude M_{0e}.

Within the single-band approximation, the Hamiltonian above can be written into a lattice model

$$\hat{H}_0 = \sum_{\alpha,\sigma\langle i,j\rangle} t_{1\alpha}\hat{c}^\dagger_{i\alpha\sigma}\hat{c}_{j\alpha\sigma} + \sum_{\alpha,\sigma\langle\langle i,j\rangle\rangle} t_{2\alpha}\hat{c}^\dagger_{i\alpha\sigma}\hat{c}_{j\alpha\sigma} + \Gamma^\alpha_z \sum_i (\hat{n}_{i\alpha\uparrow} - \hat{n}_{i\alpha\downarrow}) + \sum_i \Omega_{i\alpha}(\hat{c}^\dagger_{i\alpha\uparrow}\hat{c}_{i\alpha\downarrow} - \hat{c}^\dagger_{i\alpha\uparrow}\hat{c}_{i\alpha\downarrow} + \text{H.c.}), \quad (2)$$

where $\hat{c}_{i\alpha\sigma}$ is the annihilation operator for atoms on site i with spin σ and orbital α, $\hat{n}_{i\alpha\sigma} = \hat{c}^\dagger_{i\alpha\sigma}\hat{c}_{i\alpha\sigma}$ is the corresponding number operator, $t_{1\alpha}$ and $t_{2\alpha}$ are the spin-conserving hopping rates for nearest neighbors $\langle i,j\rangle$ and next nearest neighbors $\langle\langle i,j\rangle\rangle$, respectively, and Γ^α_z is the effective Zeeman field for the α orbital, which gives the energy shift resulting from the two-photon detuning of the corresponding Raman process. Note that Γ^α_z originates from the energy offset $\delta_{\alpha\sigma}$ between the two nuclear spin states, and is different for the two orbitals at finite external magnetic fields. While the spin-orbit coupling rate for the $|g\rangle$ orbital is a constant Ω_{ig}, that for the $|e\rangle$ orbital is a random function $\Omega_{ie} = W_{\Omega_e}\text{rand}(0,1)$. The parameters in the lattice Hamiltonian can be obtained from the continuous space Hamiltonian eq. (1) by calculating the corresponding overlap integrals of Wannier functions. In the absence of interactions, the two orbitals are decoupled, and the single-particle eigenstates within each orbital are composed of spin-up and spin-down components and usually referred as helix. Notice that while the contribution from spin-up and spin-down atoms to the $|g\rangle$ orbital helix is fixed, those for the $|e\rangle$ orbital helix are fluctuating due to the randomness of Ω_{ie}.

A key property of this system is the inter-orbital spin-exchange interactions in the clock-state manifolds. In three-dimensional space, the interaction depends on whether the orbital degrees of freedom are singlet or triplet, with the scattering lengths of the two scattering channels given by a_{s-} and a_{s+}, respectively. In a quasi-1D trapping potential and under a finite external magnetic field, the two scattering channels are coupled, and the interaction under the tight-binding approximation can be written as

$$\hat{H}_{\text{int}} = \sum_i (V_{ex}\hat{c}^\dagger_{ig\uparrow}\hat{c}^\dagger_{ie\downarrow}\hat{c}_{ie\downarrow}\hat{c}_{ig\uparrow} + \text{H.c.}) + \sum_i (U_g\hat{n}_{ig\uparrow}\hat{n}_{ig\downarrow} + U_e\hat{n}_{ie\uparrow}\hat{n}_{ie\downarrow}) + \sum_{i\sigma} U_0\hat{n}_{ig\sigma}\hat{n}_{ie\sigma}, \quad (3)$$

where U and U_0 are the Hartree-type on-site interactions, and V_{ex} is the on-site inter-orbital spin-exchange interaction. All the on-site interaction parameters $\{V_{ex}, U, U_0\}$ can be tuned via the external magnetic field through the orbital Feshbach resonance, or via the transverse trapping frequencies through the confinement-induced resonance. Due to the presence of disorder in the $|e\rangle$ orbital, all the on-site interaction parameters related to the $|e\rangle$ orbital are random in nature. Nevertheless, in the following calculation we consider a simplified setup with constant V_{ex} and U_0, and a random $U_e = W_{U_e}\text{rand}(0,1)$. In this configuration, the system corresponds to a ladder as shown in fig. 1, with one leg ($|g\rangle$) free of disorder and the other leg ($|e\rangle$) with both random spin-orbit coupling and on-site interaction. An interesting question is whether localization can take place in the disorder-free leg due to the coupling to the other leg.

Transition from thermal to localized phases. – To address the question raised above, we assume the leg with disorder ($|e\rangle$) is filled with 1/2 particle per site, while the number of particles in the disorder-free $|g\rangle$ orbital is fixed to be unity. We use ED to calculate the eigenstates for systems of length L up to 16, and extract several key indicators to investigate the localization transition. In the following discussion, we choose the hopping rate between nearest neighbors in the $|e\rangle$ orbital as energy unit $t_{1e} = 1$, and choose other parameters as $t_{2e} = 0.5$, $t_{1g} = t_{2g} = 0$, $\Omega_g = 0.5$, $\Gamma^g_z = 0$, $\Gamma^e_z = 2.0$, $U_0 = 0.5$, $U_g = 8.0$, and $V_{ex} = 4.0$. Notice that the hopping rates in the $|g\rangle$ are assumed to be zero reflecting the fact that the impurity is fixed. The two quantities that acquire randomness are assumed to be of the same intensity with $\Omega_e = W \times \text{rand}(0,1)$ and $U_e = W \times \text{rand}(0,1)$. This choice of parameters is realistic for ^{173}Yb atoms trapped in quasi-1D optical lattices near an orbital Feshbach resonance [36]. In our numerical calculation, we average over at least 3000 randomly generated parameter combinations until convergence is obtained for the means.

The first quantity of interest is the entanglement entropy $S^E = -\text{Tr}(\rho_A \ln \rho_A)$ of a subsystem A with $\rho_A = \text{Tr}_{I-A}(|\psi\rangle\langle\psi|)$ the reduced density matrix. We first cut the ladder in the middle and calculate the entanglement entropy for the left (or equivalently right) subsystem. In fig. 2 we show the mean S^E_{LR} (top) and standard deviation σ^E_{LR} (bottom) of the entanglement entropy by varying the strength of disorder W. The entanglement entropy is evaluated at an energy in the middle of the spectrum by averaging over at least 50 eigenpairs in order to reduce finite size effects.

For weak disorder, the system is in the thermal phase where the entanglement entropy follows a volume law approaching the Page value $S = (L\ln 2 - 1)/2$ of a pure random state as shown by dotted lines [37]. By increasing disorder, S^E_{LR} decreases monotonically and saturates at $S = \ln 2$ (dashed line) in the localized state. The transition from the thermal to the localized state becomes sharper with increasing system size L. The standard deviation of the entanglement entropy tends to vanish in the thermodynamic limit in the deep thermal state, which is consistent with the ETH. In the deep localized state, σ^E_{LR} also goes to zero since all states acquire the same entanglement entropy of $\ln 2$. In the middle, the standard deviation shows a diverging behavior, indicating that MBL is indeed a phase transition in the thermodynamic limit.

Next we cut the ladder system into two separate chains, and plot the mean S^E_{UD} (top) and standard deviation σ^E_{UD}

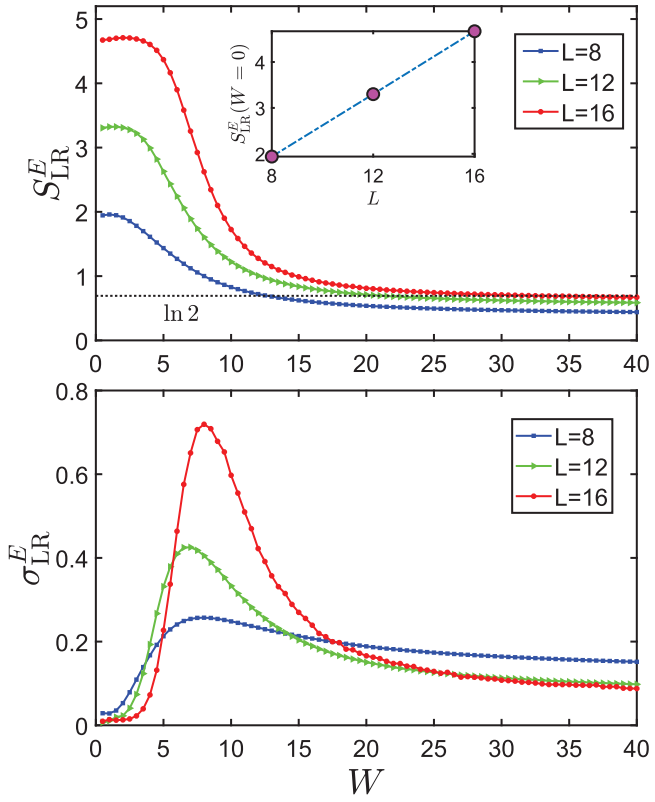

Fig. 2: (a) Mean of entanglement entropy as a function of disorder strength W. The entropy is obtained for the left (or equivalently, right) subsystem by cutting the ladder at the center, and evaluated in the middle of the spectrum. The inset shows the volume law of the entanglement entropy without disorder and the dashed line indicates the anticipated $\ln 2$ entanglement entropy in the deep MBL phase. (b) Standard deviation of the entanglement entropy as a function of disorder strength W. The thermal-to-localized transition is shown by the diverging behavior.

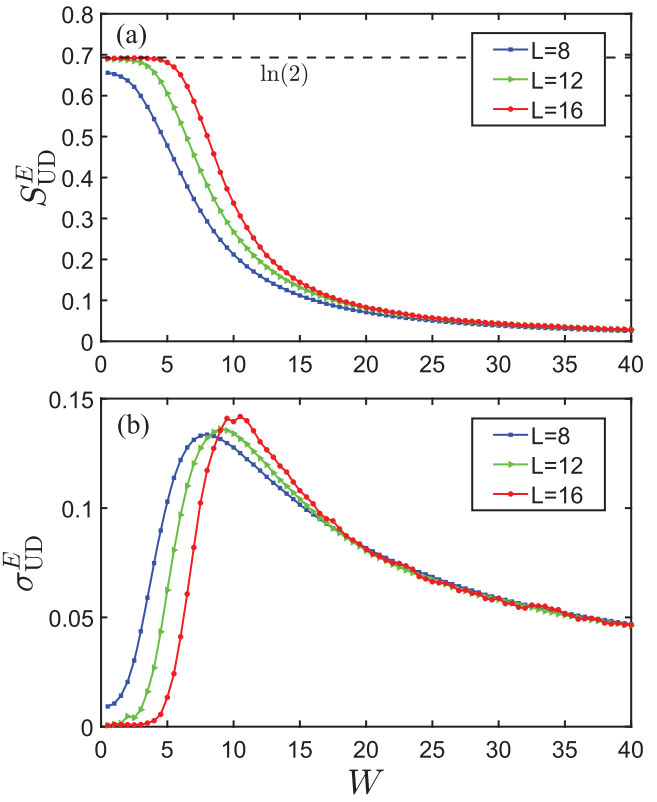

Fig. 3: (a) Mean and (b) standard deviation of the entanglement entropy of the impurity. The dashed line shows the limiting behavior of a deep thermal state of $S = \ln 2$. Parameters used here are the same as in fig. 2.

(bottom) of the entanglement entropy of the $|g\rangle$ orbital in fig. 3. From these results, we observe similar trends of variation as in fig. 2 by increasing the disorder strength from the thermal state to the localized state. Quantitatively, as the impurity in the $|g\rangle$ orbital is fixed in space, in the deep thermal state the system tends to a cat state with the impurity of either spin-up or spin-down, hence acquires an entanglement entropy of $S = \ln 2$ as indicated by the dashed line in fig. 3. In the deep localized state, however, the impurity is fixed at one specific spin state, leading to a vanishing entropy in this limiting case.

Another important indicator for the MBL transition is the average ratio between the smallest and the largest adjacent energy gaps, $r_n = \min[\delta^E_n, \delta^E_{n-1}]/\max[\delta^E_n, \delta^E_{n-1}]$ [6]. Here, $\{E_n\}$ is the ordered list of energy levels and $\delta^E_n = E_n - E_{n-1}$ is the separation between two adjacent eigenstates. As shown in fig. 4, in the thermal phase where the level spacing exhibits a Wigner-Dyson distribution, the average ratio is $\langle \bar{r} \rangle_{\rm dis} \approx 0.5307$, while in the localized phase where the level spacing exhibits a Poisson distribution,

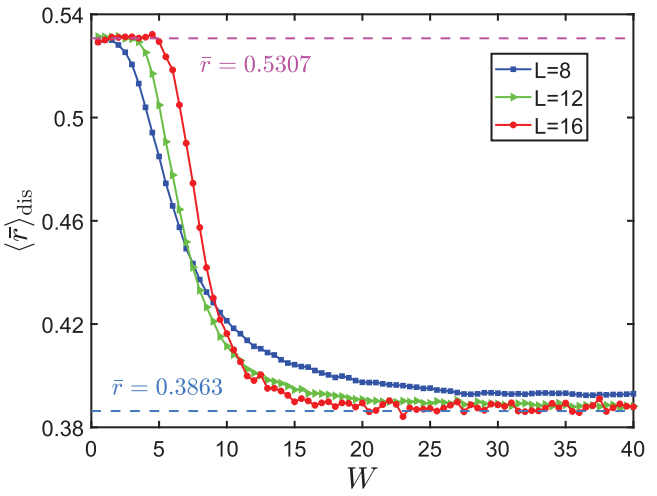

Fig. 4: Average ratio of adjacent energy gaps as a function of the disorder strengths. Dashed lines show the limiting value for the deep thermal and localized states where spectra acquire Wigner-Dyson (0.5307) and Poisson (0.3863) distributions, respectively. Parameters used here are the same as in fig. 2.

the average ratio is $\langle \bar{r} \rangle_{\rm dis} = 2\ln 2 - 1 \approx 0.3863$ [38]. The variation becomes sharper with increasing system size, indicating the MBL transition in the thermodynamic limit.

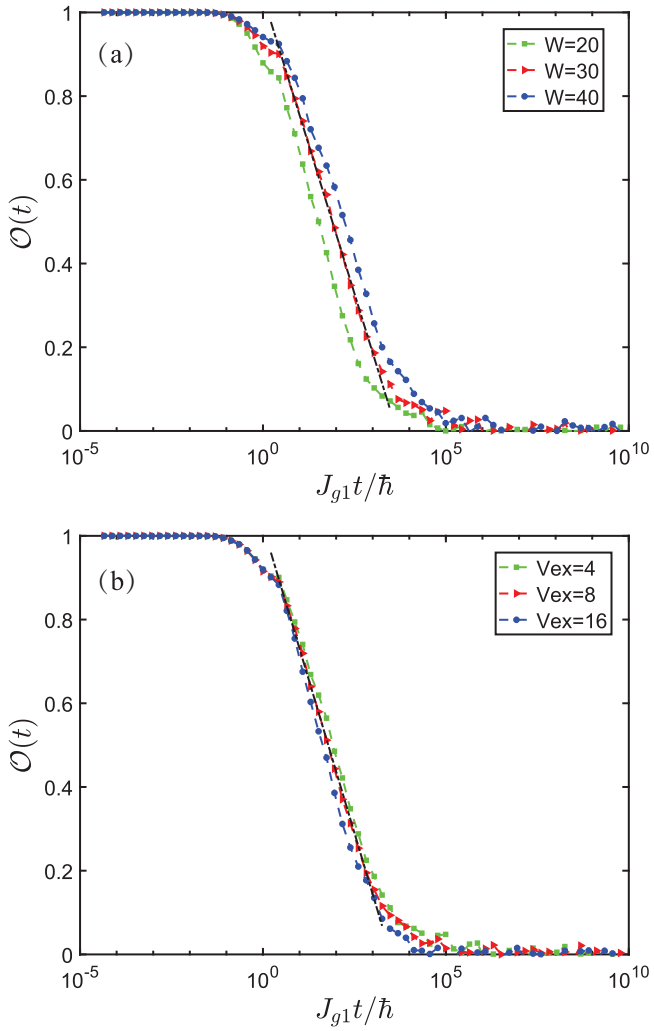

Fig. 5: Time evolution of OTOC in the MBL state by varying (a) disorder strengths with $V_{ex} = 4.0$ and (b) spin-exchange interaction with $W = 30$. The results are scaled to drop from unity in short time. The horizontal axis is in the logarithmic scale to show the power-law behavior (dashed line) at intermediate time. In this calculation, we choose a system size of $L = 8$. Other parameters are the same as in fig. 2.

Finally, we study the evolution of OTOC in the MBL phase, as defined by

$$\mathcal{O}(t) \equiv \langle \hat{A}^\dagger(t)\hat{B}^\dagger(0)\hat{A}(t)\hat{B}(0)\rangle, \tag{4}$$

where $\hat{S}(t) = e^{i\hat{H}t}\hat{S}e^{-i\hat{H}t}$ is the time-dependent operator for $\hat{S} = (\hat{A}, \hat{B})$, and $\langle \dots \rangle$ denotes the expectation value for the ground state at zero temperature. OTOC is a commonly used quantity to characterize the chaotic behavior of a quantum system. The exponential deviation of OTOC defines the Lyapunov exponent [39,40]. Previous studies show that the MBL phase is not chaotic, and the time evolution of OTOC therein presents a power-law decay instead of an exponential deviation [19,20,41–44]. It is also suggested that OTOC can serve as an indicator to distinguish a MBL state from an AL state. While the OTOC remains a constant over time in the AL phase, it decreases in the MBL phase accompanying a logarithmic growth of entropy [20].

For our system, we take the operators in eq. (4) as a linear combination of creation and annihilation operators at adjacent sites $\hat{A} = (c_i + c_i^\dagger)$ and $\hat{B} = (c_{i+1} + c_{i+1}^\dagger)$. In fig. 5, we show time evolution of OTOC for the MBL phase for various disorder strengths and spin-exchange interactions. The results are averaged over half lattice sites at the center and over 3000 random configurations to achieve convergence. In all cases, we observe that after a certain amount of time $t \sim \hbar/t_1$ OTOC starts to deviate from unity, as in clear contrast to the AL state where OTOC remains 1. For intermediate time, the decay is in power-law instead of exponential, showing a distinctive behavior in comparison to a thermal state. The power-law exponent, as indicated by dashed lines in fig. 5, is not a universal value but changes slightly for different choice of parameters. For long enough time $t \to \infty$, OTOC tends to zero.

Summary. – We study the thermal to many-body localization transition in generalized Kondo lattice, where a 1D Hubbard chain with disordered spin-orbit coupling and on-site interaction coupled to a fixed impurity of spin 1/2 via spin-exchange interactions. We find that for large enough disorder strength, the system undergoes a transition from thermal to localized state, during which the entanglement entropy shows an abrupt change. This result shows that although the subsystem of the impurity is free of disorder, it can still be localized in spin space by the coupling with the Hubbard chain. The localized transition can also be characterized by the average ratio between the smallest and the largest adjacent energy gaps, which shows that the spectrum changes from a Wigner-Dyson distribution in the thermal state to a Poisson distribution in the localized state. We also investigate the OTOC in the many-body localized phase, and find distinctive features in comparison to either the thermal state or the AL state. The theoretical model we discussed here can be realized in ultracold quantum gases of alkaline-earth–like atoms near an orbital Feshbach resonance in a 1D optical lattice.

* * *

This work is supported by the National Key R&D Program of China (Grant No. 2018YFA0306501), the National Natural Science Foundation of China (Grant Nos. 11434011, 11522436, 11704029, 11774425), the Beijing Natural Science Foundation (Grant No. Z180013), and the Research Funds of Renmin University of China (Grants No. 16XNLQ03 and No. 18XNLQ15).

REFERENCES

[1] Anderson P. W., *Phys. Rev.*, **109** (1958) 1492.
[2] Abrahams E., Anderson P. W., Licciardello D. C. and Ramakrishnan T. V., *Phys. Rev. Lett.*, **42** (1979) 673.

[3] Altshuler B. L., Gefen Y., Kamenev A. and Levitov L. S., *Phys. Rev. Lett.*, **78** (1997) 2803.
[4] Gornyi I. V., Mirlin A. D. and Polyakov D. G., *Phys. Rev. Lett.*, **95** (2005) 206603.
[5] Basko D. M., Aleiner I. L. and Altshuler B. L., *Ann. Phys.*, **321** (2006) 1126.
[6] Oganesyan V. and Huse D. A., *Phys. Rev. B*, **75** (2007) 155111.
[7] Žnidarič M., Prosen T. and Prelovšek P., *Phys. Rev. B*, **77** (2008) 064426.
[8] Pal A. and Huse D. A., *Phys. Rev. B*, **82** (2010) 174411.
[9] Khatami E., Rigol M., Relano A. and Garcia-Garcia A. M., *Phys. Rev. E*, **85** (2012) 050102(R).
[10] Bardarson J. H., Pollmann F. and Moore J. E., *Phys. Rev. Lett.*, **109** (2012) 017202.
[11] Panda R. K., Scardicchio A., Schulz M., Taylor S. R. and Žnidarič M., *EPL*, **128** (2019) 67003.
[12] Yao N. Y., Laumann C. R., Cirac J. I., Lukin M. D. and Moore J. E., *Phys. Rev. Lett.*, **117** (2016) 240601.
[13] Huse D. A., Nandkishore R., Pietracaprina F., Ros V. and Scardicchio A., *Phys. Rev. B*, **92** (2015) 14203.
[14] Bai X.-D., Wang J., Liu X.-J., Xiong J., Deng F.-G. and Hu H., *Phys. Rev. A*, **98** (2018) 23627.
[15] Kondov S. S., McGehee W. R., Xu W. and DeMarco B., *Phys. Rev. Lett.*, **114** (2015) 083002.
[16] Schreiber M., Hodgman S. S., Bordia P., Lüschen H. P., Fischer M. H., Vosk R., Altman E., SchneiderU. and Bloch I., *Science*, **349** (2015) 842.
[17] Bordia P., Lüschen H. P., Hodgman S. S., Schreiber M., Bloch I. and Schneider U., *Phys. Rev. Lett.*, **116** (2016) 140401.
[18] Smith J., Lee A., Richerme P., Neyenhuis B., Hess P. W., Hauke P., Heyl M., Huse D. A. and Monroe C., *Nat. Phys.*, **12** (2016) 907.
[19] Serbyn M., Papić Z. and Abanin D. A., *Phys. Rev. Lett.*, **111** (2013) 127201.
[20] Fan R., Zhang P., Shen H. and Zhai H., *Sci. Bull.*, **62** (2017) 707.
[21] Rigol M., Dunjko V. and Olshanii M., *Nature*, **452** (2008) 854.
[22] Rigol M., *Phys. Rev. Lett.*, **103** (2009) 100403.
[23] Rigol M., *Phys. Rev. A*, **80** (2009) 053607.
[24] Santos L. F. and Rigol M., *Phys. Rev. E*, **82** (2010) 031130.
[25] Neuenhahn C. and Marquardt F., *Phys. Rev. E*, **85** (2012) 060101.
[26] Khatami E., Pupillo G., Srednicki M. and Rigol M., *Phys. Rev. Lett.*, **111** (2013) 050403.
[27] Steinigeweg R., Herbrych J. and Prelovšek P., *Phys. Rev. E*, **87** (2013) 012118.
[28] Beugeling W., Moessner R. and Haque M., *Phys. Rev. E*, **89** (2014) 042112.
[29] Kim H., Ikeda T. N. and Huse D. A., *Phys. Rev. E*, **90** (2014) 052105.
[30] Sorg S., Vidmar L., Pollet L. and Heidrich-Meisner F., *Phys. Rev. A*, **90** (2014) 033606.
[31] Moure N., Haas S. and Kettemann S., *EPL*, **111** (2015) 27003.
[32] De Luca A. and Scardicchio A., *EPL*, **101** (2013) 37003.
[33] Rigol M., *Phys. Rev. Lett.*, **112** (2014) 170601.
[34] Tang B., Iyer D. and Rigol M., *Phys. Rev. B*, **91** (2015) 161109(R) .
[35] Zhou X., Pan J.-S., Liu Z.-X., Zhang W., Yi W., Chen G. and Jia S., *Phys. Rev. Lett.*, **119** (2017) 185701.
[36] Song B., He C., Zhang S., Hajiyev E., Huang W., Liu X.-J. and Jo G.-B., *Phys. Rev. A*, **94** (2016) 061604.
[37] Page D. N., *Phys. Rev. Lett.*, **71** (1993) 1291.
[38] Atas Y. Y., Bogomolny E., Giraud O. and Roux G., *Phys. Rev. Lett.*, **110** (2013) 084101.
[39] Shenker S. H. and Stanford D., *JHEP*, **03** (2014) 067.
[40] Larkin A. I. and Ovchinnikov Y. N., *Sov. Phys. JETP*, **28** (1969) 1200.
[41] Nandkishore R. and Huse D. A., *Annu. Rev. Condens. Matter Phys.*, **6** (2015) 15.
[42] Altman E. and Vosk R., *Annu. Rev. Condens. Matter Phys.*, **6** (2015) 383.
[43] Huse D. A., Nandkishore R. and Oganesyan V., *Phys. Rev. B*, **90** (2014) 174202.
[44] Vosk R. and Altman E., *Phys. Rev. Lett.*, **110** (2013) 067204.